THE ASTROPHYSICAL JOURNAL, 495:L23–L26, 1998 March 1

INFRARED IMAGING AND SPECTROSCOPY OF THE HELIX WITH ISOCAM[1]

P. COX,[2] F. BOULANGER,[2] P. J. HUGGINS,[3] A. G. G. M. TIELENS,[4] T. FORVEILLE,[5] R. BACHILLER,[6] D. CESARSKY,[2] A. P. JONES,[2] K. YOUNG,[7] P. R. ROELFSEMA,[4] AND J. CERNICHARO[8]

Received 1997 October 31; accepted 1997 December 29; published 1998 February 13

ABSTRACT

We report infrared images of the Helix Nebula centered at 6.9 μm (LW2 filter) and 15 μm (LW3 filter) obtained with ISOCAM on board the *Infrared Space Observatory* (*ISO*). Three fields were also measured using the ISOCAM circular variable filter (CVF). The CVF data show that the 5–16.6 μm spectrum is dominated by the pure ($v = 0$–0) rotational lines of molecular hydrogen from the $S(7)$ to the $S(2)$ transitions. The strong $S(5)$ H_2 line accounts for most of the emission detected in the LW2 filter. The only atomic lines detected are [Ne II] 12.81 μm and [Ar III] 8.99 μm, which are weak, and [Ne III] 15.55 μm, which is strong and accounts for most of the emission in the LW3 filter. No emission bands or continuum of small dust particles are detected despite the carbon richness of the Helix Nebula.

The H_2 emission traces the individual cometary globules of the molecular envelope of the nebula, whereas the [Ne III] emission is distributed along this envelope toward the inner regions of the ionized cavity. The intensities of H_2 rotational lines are accurately predicted using a rotational temperature of 900 ± 50 K and column densities of $\sim 3 \times 10^{18}$ cm^{-2}. The total luminosity in the H_2 lines $\sim 4\ L_\odot$ (6% of the star luminosity) is much higher than predicted for photodissociation regions. The significant absence of mid-infrared dust features indicates that in this evolved planetary nebula, the molecular-sized dust particles might have been destroyed by the exposure to the radiation field from the central hot star.

Subject headings: infrared: ISM: lines and bands — planetary nebulae: individual (NGC 7293) — stars: AGB and post-AGB — stars: mass loss

1. INTRODUCTION

The Helix (NGC 7293, PK 36−57.1) is one of the nearest planetary nebulae (PNe) with an estimated distance of ~160 pc (Cahn et al. 1992). The optical appearance of the nebula consists of the well-known double-ring structure, approximately 10′ in diameter (Warner & Rubin 1975; Walsh & Meaburn 1987). Similar ring structures are found in the massive envelope of molecular gas associated with the Helix, which forms a large broken shell surrounding the ionized cavity (Healy & Huggins 1990; Kastner et al. 1996). This molecular envelope is very inhomogeneous (Forveille & Huggins 1991; Young et al. 1997) and consists of numerous dense condensations that are associated with the cometary globules (Huggins et al. 1992) seen at optical wavelengths (Meaburn et al. 1992; O'Dell & Handron 1996). The variable extinction across the face of the nebula (Warner & Rubin 1975) and the extinction of background [O III] 5007 Å emission in the globules (Meaburn et al. 1992) both indicate the presence of dust in the Helix. The infrared emission was mapped by the *IRAS* satellite and has been studied by Leene & Pottasch (1987).

In this Letter, we report imaging of the Helix at mid-infrared wavelengths using the ISOCAM camera (Cesarsky et al. 1996) on board *ISO* (Kessler et al. 1996). The observations reveal at unprecedented angular resolution (6″) and sensitivity (mJy level) the mid-infrared emission in an evolved PN. Additional spectro-imagery using the ISOCAM CVF reveals the composition of the mid-infrared emission.

2. OBSERVATIONS AND RESULTS

The images were taken in 1996 May in the LW2 (5–8.5 μm) and LW3 (12–18 μm) filters. With a pixel size of 6″, the camera field is 3′ × 3′ (32 × 32 pixels). The extent of the optical nebula (14′ × 14′) was covered with a raster map of 15 × 15 frames with an overlap of half a frame for each raster position. The integration time per frame and the total integration time were, respectively, 8.4 and 5052 s for LW2 and 25.2 and 8205 s for LW3.

The images have been reduced following Abergel et al. (1996). In addition, an interactive method (to be reported elsewhere) has been applied that makes use of the data redundancy (each point in the sky is observed by different pixels of the camera) to identify long-term glitches and remove the time-correlated noise. The calibration is based on the system response value given in the ISOCAM observer's manual.

Three fields were also observed in 1997 April using the ISOCAM CVF: two in the northern part of the molecular envelope and one toward the western rim. A pixel size of 6″ was used, yielding a total field of view of 3′ × 3′. Complete scans of the long-wavelength CVF were obtained: the LW-CVF2 from 16.6 to 9.0 μm and the LW-CVF1 from 9.4 to 5.0 μm. The effective spectral resolution is ~40. The data reduction and photometric calibration were carried out following Boulanger et al. (1996). In addition, we have used calibration data to correct for the stray light associated with the zodiacal emission.

[1] Based on observations with *ISO*, an ESA project with instruments funded by ESA Member States (especially the PI countries: France Germany, the Netherlands, and the United Kingdom) and with the participation of ISAS and NASA.

[2] Institut d'Astrophysique Spatiale, Université de Paris XI, 91405 Orsay, France.

[3] Physics Department, New York University, 4 Washington Place, New York, NY 10003.

[4] SRON, P.O. Box 800, 9700 AV Groningen, The Netherlands.

[5] Observatoire de Grenoble, B. P. 53X, 38041 Grenoble Cedex, France.

[6] Observatorio Astronómico Nacional (IGN), Apdo 1143, 28800 Alcalá de Henares, Spain.

[7] Smithsonian Astrophysical Observatory, 60 Garden Street MS 78, Cambridge, MA 02138.

[8] Instituto de Estructura de la Materia, CSIC, Serrano 123, E-28006 Madrid, Spain.

2.1. *LW2 and LW3 Imaging*

The ISOCAM LW2 and LW3 images of the Helix Nebula are displayed in Figure 1 (Plate L3). The image in the LW2 filter (around 6.9 μm) shows highly structured emission where the globules, filaments, and wisps of the nebula are clearly seen. The inner ring is significantly weaker than the outer ring. The overall appearance of the LW2 emission is similar to the morphology of the optical [O I] emission (Warner & Rubin 1975). The halo and the emission in the polar regions, present at low level in optical images (Walsh & Meaburn 1987), are well detected in the LW2 image with intensities only factors of 2–3 lower than for the inner structures. At lower levels, the LW2 emission shows numerous rays extending outward radially from the edge of the outer ring. These rays link the outer ring with the halo in the northeast. In contrast, there is no LW2 emission in the inner cavity.

The LW3 emission (around 15 μm) is morphologically very different from the LW2 image. Its distribution is much smoother and more concentrated toward the center. It is equally strong in the outer and inner rings, and the low-level emission fills the inner cavity and peaks around the position of the central star.

2.2. *Spectro-imagery*

The 5–16.6 μm CVF spectra in the western rim show a series of emission lines on a continuum (Fig. 2). This continuum is remarkably well fitted by the zodiacal light spectrum from Reach et al. (1996) (see Fig. 2). We also estimated the contribution of the zodiacal light using the Diffuse Infrared Background Experiment (DIRBE) data for the ecliptic coordinates and solar elongation of the Helix observations, and we found that the derived amplitude is much less than the absolute calibration of ISOCAM (~15%). Hence, any mid-infrared dust continuum from the Helix can at most be 15% of the zodiacal light, i.e., less than 4 MJy sr^{-1} at 15 μm. After subtraction of the zodiacal contribution, the CVF spectra are dominated by the series of the pure ($v = 0$–0) rotational lines of molecular hydrogen from the $S(7)$ to the $S(2)$ transitions. In addition, there is weak [Ne II] and strong [Ne III] emission and also weak [Ar III] toward the [Ne III] peak (Fig. 3 [Pl. L4]). No other atomic lines are detected. Finally, no dust emission bands are present in the CVF spectra, including the PAH bands at 6.2, 7.7, 8.6, and 11.3 μm, which usually dominate the spectra of young carbon-rich PNe—see, e.g., Beintema et al. (1996).

Line images have been extracted from the CVF observations to show the distribution of molecular and ionized gas in the western rim. Figure 3 displays the distribution of the emission in the H_2 $S(5)$ and $S(3)$ lines compared with that of the [Ne III] 15.5 μm line. The H_2 emission extends along a southeast-northwest direction and shows a complex structure with distinct peaks of emission, matching the structures seen in the millimeter CO emission (Young et al. 1997). The peaks in the $S(3)$ and $S(5)$ emission are different, indicating that the rotational temperature varies slightly from structure to structure. The [Ne III] emission is smoother, clearly separated from the H_2, and peaks in the direction of the ionized cavity. Similar results have been found for the northern fields, and these will be discussed elsewhere.

3. DISCUSSION

The ISOCAM data on the Helix allow a detailed study of both the molecular and ionized gas in this evolved PN. The spectro-imaging results demonstrate that, in three fields, the mid-infrared emission is entirely caused by molecular hydrogen and neon lines. No dust bands are detected, and there is no continuum emission. We believe that these results apply to the entire nebula. The LW2 map is thus an image of the H_2 emission from the $S(7)$ to $S(4)$ lines, which explains its similarity to the optical [O I] emission noted previously. The LW3 map is mostly a result of the [Ne III] 15.5 μm line, which accounts for its similarity to the [O III] or Hα images (Warner & Rubin 1975)—note that the $S(1)$ line of H_2 is within the LW3 filter at the long wavelength edge of the passband. The six rotational lines of H_2 provide basic information on the excitation of the molecular hydrogen in the Helix, and the absence of any dust signature (emission bands or continuum) indicates that small grains have been destroyed in this evolved PN. In the following, we address both issues in detail.

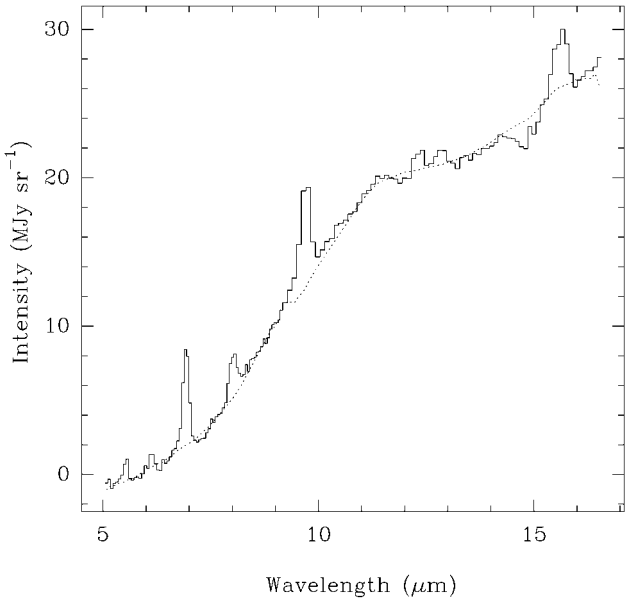

FIG. 2.—Full CVF spectrum toward the peak of the H_2 $S(5)$ emission in the western rim of the Helix Nebula (see Fig. 3). The dashed line displays the zodiacal emission. The feature at about 14.5 μm is caused by residual memory effects, after a cosmic-ray hit.

3.1. *Molecular Hydrogen Excitation*

The H_2 excitation diagram for the $S(5)$ peak of the western rim is shown in Figure 4. The statistical weights used in Figure 4 include a factor of 3 for ortho-H_2 and 1 for para-H_2. The good temperature fit confirms a posteriori that the adopted ortho-para ratio is close to 3. The H_2 excitation diagram shows that at the $S(5)$ peak of the western rim, the molecular hydrogen is well characterized by a single temperature of $T_{\rm rot} \sim 900 \pm 50$ K up to energies of about 7500 K. Comparable temperatures are derived toward the other peaks. The inferred column density of warm H_2 is $\sim 3 \times 10^{18}$ cm^{-2}, and the total intensity of the observed H_2 lines is 2.3×10^{-4} ergs cm^{-2} s^{-1} sr^{-1}. The single excitation temperature implies also that the density of the emitting gas is well in excess of the critical density of the highest level observed, i.e., $n(H_2) \geq 10^5$ cm^{-3}.

The far-UV radiation (within the wavelength range of H_2 absorption lines that can lead to photodissociation, 921–1120 Å) at $\theta \sim 4'$ from the central star (the distance of the shell) is estimated to be $\chi \sim 6$ (in units of the interstellar radiation field as given by Habing 1968) for the adopted distance of 160 pc and a central star luminosity and temperature of $L = 60\ L_\odot$

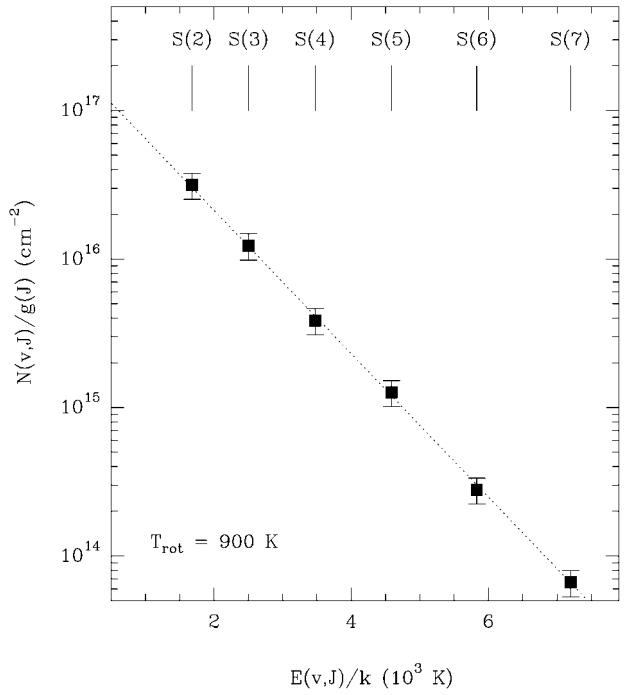

FIG. 4.—H_2 excitation diagram for the peak in the H_2 $S(5)$ emission of the western rim showing a plot of the natural logarithm of the column density, corrected for the statistical weight, in the upper level of each H_2 transition vs. the energy of that level, E_u. The dashed line represents a single temperature fitted to the data with $T_{rot} = 900 \pm 50$ K.

and $T = 120,000$ K, respectively (Bohlin et al. 1982). For such a low radiation field, the far-UV mean intensity is 8×10^{-4} ergs cm^{-2} s^{-1} sr^{-1}. Hence, the observed H_2 emission (at the peak) corresponds to ~30% of the incident radiative energy. From the integrated flux in the LW2 map (2.5×10^{-12} W m^{-2}) and the excitation diagram (Fig. 4), the total luminosity in the H_2 lines is estimated to be ~4 $L_\odot$, i.e., 6% of the stellar luminosity. This is extremely high compared with what is normally observed in photodissociation regions (PDR), where the H_2 lines represent only a fraction of a percent of the available radiative energy as, e.g., in the Orion Bar (Parmar, Lacy, & Achtermann 1991) or S140 (Timmermann et al. 1996). For radiation fields of $\chi \sim 6$, the calculated fluorescence emission is typically 2×10^{-7} ergs s^{-1} cm^{-2} sr^{-1} for the $S(5)$ H_2 line (using the model of Burton, Hollenbach, & Tielens 1992), i.e., 2 orders of magnitude lower than observed (~10^{-4} ergs s^{-1} cm^{-2} sr^{-1}). Also at these low-incident far-UV fields, the gas temperature predicted by PDR models (20–50 K; Hollenbach, Takahashi, & Tielens 1991) is much too low to explain the observed pure rotational emission. Finally, the absence of mid-infrared dust features introduces a severe difficulty in the H_2 excitation through UV radiation, since it suppresses the important photoelectric heating of the gas by small grains (Bakes & Tielens 1994).

X-rays are a potential source of gas heating by photoionizing the atoms and molecules and depositing a fraction of the primary and secondary electron energy into heat (Maloney, Hollenbach, & Tielens 1996 and references therein). With an X-ray luminosity of 1.3×10^{33} ergs s^{-1} (Leahy, Zhang, & Kwok 1994) and a physical size of the envelope of 6×10^{17} cm (4′), the X-ray intensity is well below the far-UV flux and the flux observed in the pure rotational lines of H_2. The role of X-rays is thus negligible.

Another possibility is excitation by shocks. C-shocks are unlikely because the magnetic field in the Helix Nebula is expected to be very weak. For nondissociative J-shocks with a shock velocity $v_s \sim 10$ km s^{-1} and a preshock density of 10^6 cm^{-3}, the calculated temperature and column density of the shocked H_2 gas are 1000 K and 6×10^{18} cm^{-2}, respectively (Burton et al. 1992), consistent with the observations. Dissociative J-shocks will produce column densities that are too high (~10^{21} cm^{-2}) and temperatures that are too low (~400 K) compared with the observations and therefore are ruled out. The shock excitation of the H_2 can be placed in the context of the interacting wind model, where the fast wind from the central star sweeps up the slowly moving AGB wind material. However, the luminosity in the H_2 lines (~4 $L_\odot$) implies a very high ratio of mechanical-to-radiative luminosity. The required mass-loss rate (3×10^{-8} $M_\odot$ yr^{-1}) and wind velocity (1000 km s^{-1}) are similar to the values suggested by Leahy et al. (1994) on the basis of the X-ray emission. However, the X-ray source is unresolved (less than 15″), which is unexpected within the framework of the interacting wind model. Moreover, there is no direct evidence for P Cygni profiles in the spectrum of the central star (Cerruti-Sola & Perinotto 1985).

In summary, despite the fact that the globules in the Helix show a typical PDR morphology (an ensemble of dense globules with ionized surfaces and C I/CO layers), the far-UV radiation from the central star appears to be much too low to account for the H_2 line intensities and the high temperatures (900 K) that are observed. Nondissociative J-shocks are able to reproduce the observed temperature and column densities. However, shocks imply a very high mechanical luminosity, and there is no strong evidence in the Helix for a stellar wind with the required mass-loss rate and velocity. The influence of the extreme-UV radiation from the star could perhaps play an important role in heating the H_2 if the molecular hydrogen survives up to the ionization front. Future observations should help to further constrain the excitation of the molecular hydrogen in the Helix. In particular, measurements of high-v rovibrational H_2 lines will test the importance of fluorescence, observations of the fine-structure lines of [C II] and [O I] will allow a better understanding of the interface regions, and measuring high-J CO lines will assess if shocks are important since, in this case, according to models the CO lines should account for ~10% of the total infrared luminosity.

3.2. *Dust Destruction*

The C/O ratio in the Helix has not been measured, but evidence strongly suggests that the envelope of the Helix is carbon rich. First, the abundances of molecular species such as CN, HCN, HNC, and HCO^+ are comparable with the abundances measured in C-rich nebulae (Bachiller et al. 1997). Second, the high abundance of neutral carbon (C I/CO ~ 6) that has been measured toward the western rim is only expected in carbon-rich environments (Young et al. 1997). In view of the carbon richness of the Helix molecular envelope, the absence of the familiar PAH emission features in the CVF spectra is surprising. The upper limit on the intensity of the PAH features is 1 order of magnitude lower than in PDRs of comparable χ-value such as Ophiucus (Boulanger et al. 1996). Thus, in the Helix, PAHs are underabundant not only within the ionized gas but also in the gas layers shielded from Lyman continuum photons. This is unlike what is observed in well-known H II region/molecular cloud interfaces such as M17 (Giard et al. 1994).

The absence of PAH emission bands in the mid-infrared spectra implies that no molecular-sized dust particles are present in the envelope of this evolved PN. A possibility is that

the small particles have been destroyed by exposure to the strong radiation field of the central star in the first few thousands years of the PN phase. In any case, the Helix will not enrich the interstellar medium in PAHs or small grains. It would be of interest to study other evolved carbon-rich PNe and check if this result is general, in which case an efficient process of producing small grains must be active in the interstellar medium to account for their ubiquitous presence in space.

This work was supported in part by NSF grant AST-96-17941 (to P. J. H.).

REFERENCES

Abergel, A., et al. 1996, A&A, 315, L329
Bachiller, R., Forveille, T., Huggins, P. J., & Cox, P. 1997, A&A, 324, 1123
Bakes, E. L. O., & Tielens, A. G. G. M. 1994, ApJ, 427, 822
Beintema, D. A., et al. 1996, A&A, 315, L369
Bohlin, R. C., Harrington, J. P., & Stecher, T. P. 1982, ApJ, 252, 635
Boulanger, F., et al. 1996, A&A, 315, L325
Burton, M. G., Hollenbach, D. J., & Tielens, A. G. G. M. 1992, ApJ, 399, 563
Cahn, J. H., Kaler, J. B., & Stanghellini, L. 1992, A&AS, 94, 399
Cerruti-Sola, M., & Perinotto, M. 1985, ApJ, 291, 237
Cesarsky, C., et al. 1996, A&A, 315, L32
Forveille, T., & Huggins, P. J. 1991, A&A, 248, 599
Giard, M., Bernard, J. P., Lacombe, F., Normand, P., & Rouan, D. 1994, A&A, 291, 239
Habing, H. J. 1968, Bull. Astron. Inst. Netherlands, 19, 421
Healy, A. P., & Huggins, P. J. 1990, AJ, 100, 511
Hollenbach, D. J., Takahashi, T., & Tielens, A. G. G. M. 1991, ApJ, 377, 192
Huggins, P. J., Bachiller, R., Cox, P., & Forveille, T. 1992, ApJ, 401, L43
Kastner, J. H., Weintraub, D. A., Gatley, I., & Merrill, K. M. 1996, ApJ, 462, 777
Kessler, M., et al. 1996, A&A, 315, L1
Leahy, D. A., Zhang, C. Y., & Kwok, S. 1994, ApJ, 422, 205
Leene, A., & Pottasch, S. 1987, A&A, 173, 145
Maloney, P. R., Hollenbach, D. J., & Tielens, A. G. G. M. 1996, ApJ, 466, 561
Meaburn, J., Walsh, J. R., Clegg, R. E. S., Walton, N. A., Taylor, D., & Berry, D. S. 1992, MNRAS, 255, 177
O'Dell, R. R., & Handron, K. D. 1996, AJ, 111, 1630
Parmar, P. S., Lacy, J. H., & Achtermann, J. M. 1991, ApJ, 372, L25
Reach, W. T., et al. 1996, A&A, 315, L381
Timmermann, R., Bertoldi, F., Wright, C. M., Drapatz, S., Draine, B. T., Haser, L., & Sternberg, A. 1996, A&A, 315, L281
Walsh, J. R., & Meaburn, J. 1987, MNRAS, 224, 885
Warner, J. W., & Rubin, V. C. 1975, ApJ, 198, 593
Young, K., Cox, P., Huggins, P. J., Forveille, T., & Bachiller, R. 1997, ApJ, 482, L101

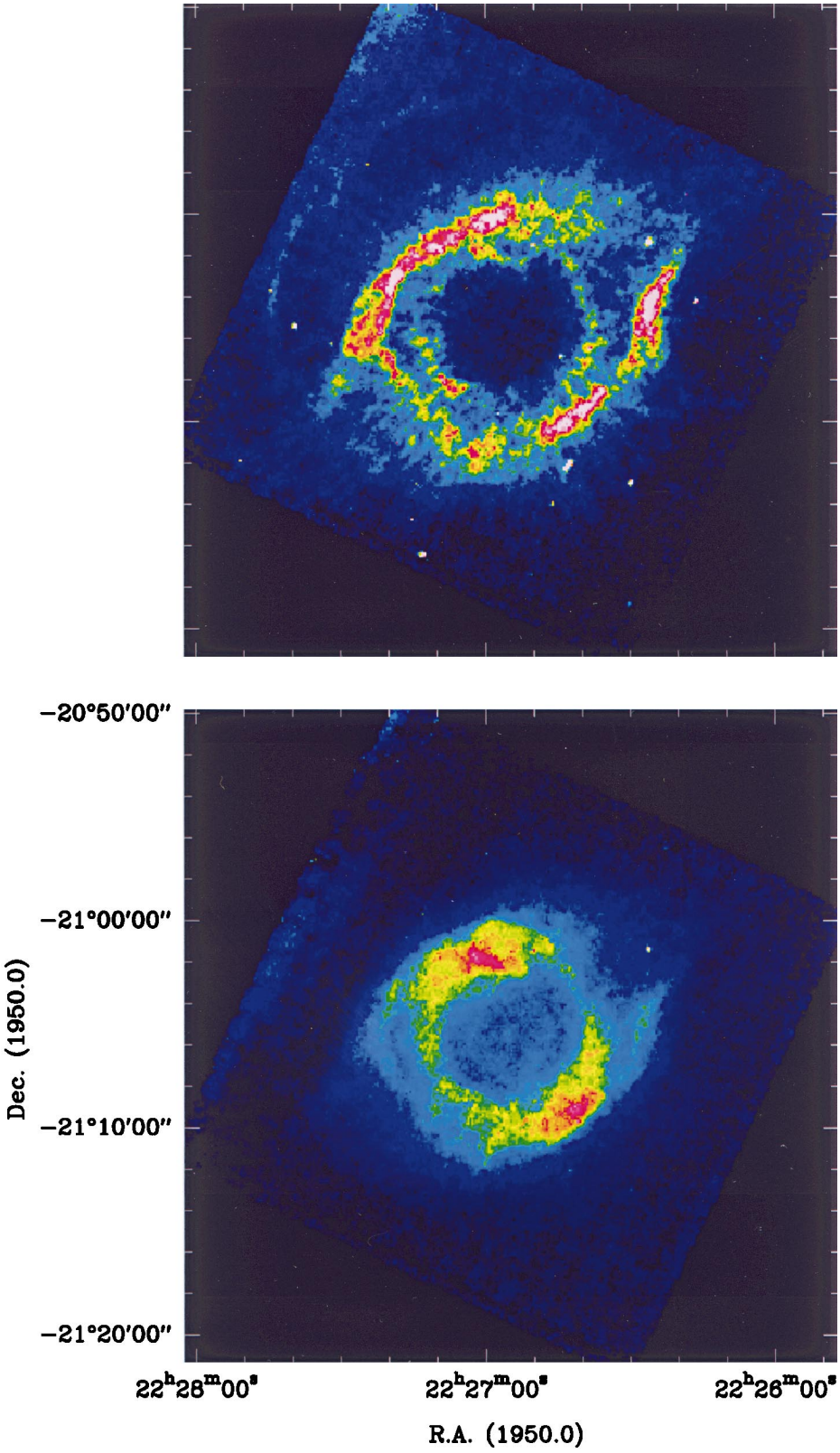

FIG. 1.—ISOCAM maps of the Helix Nebula in the LW2 filter (5.0–8.5 μm) (*upper panel*) and the LW3 filter (12.0-18.0 μm) (*lower panel*). The angular resolution of the ISOCAM images is 6″. The maximum nebular emission is 2.5 MJy sr^{-1} in both images.

Cox et al. (see 495, L24)

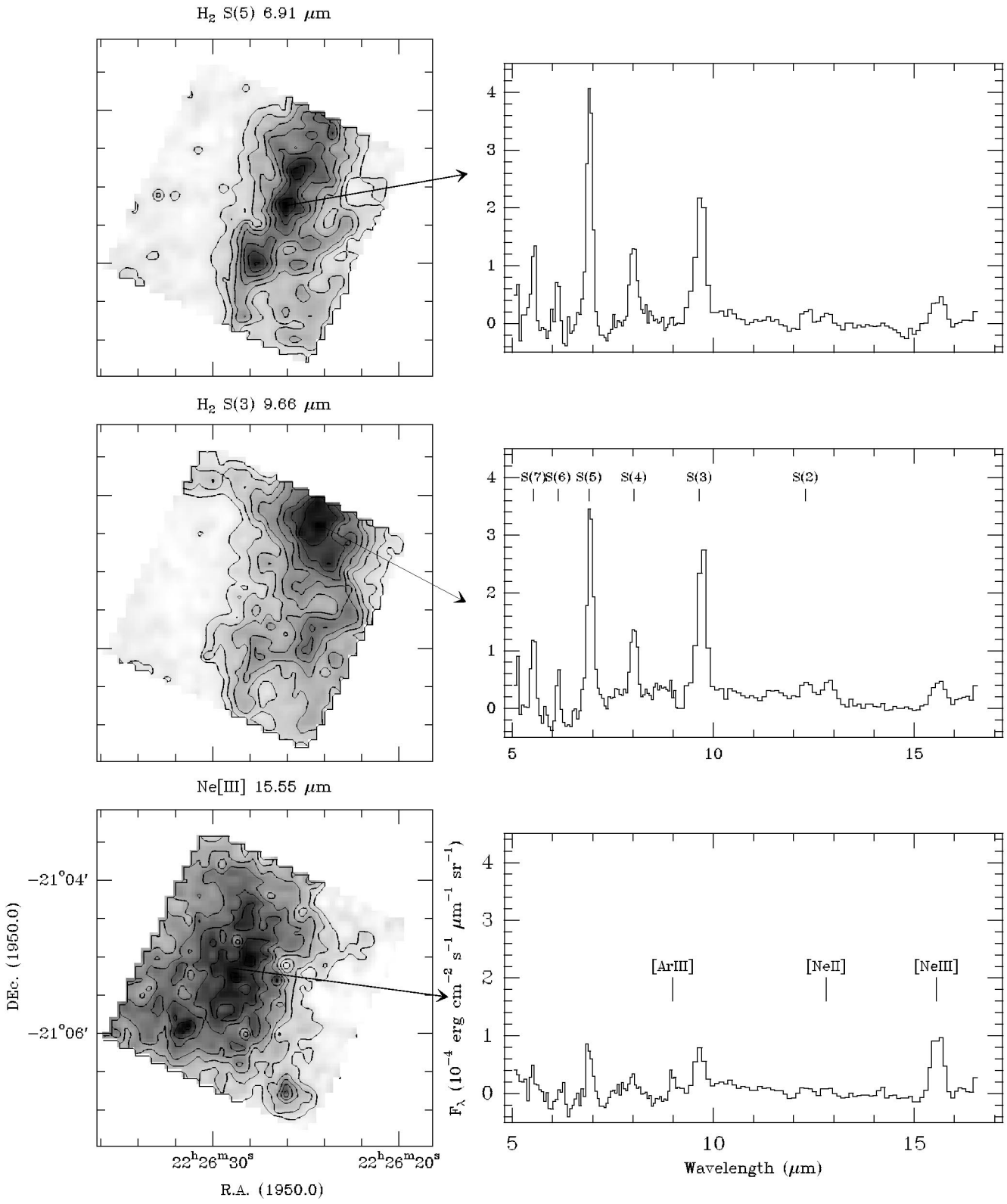

FIG. 3.—Distribution of the emission in the H_2 $S(5)$ and $S(3)$ lines, and the [Ne III] line in the western rim of the Helix Nebula. The contours are from 2×10^{-5} to 9×10^{-5} in steps of 2×10^{-5} ergs cm^{-2} s^{-1} sr^{-1}. Also shown are full CVF spectra toward the H_2 and [Ne III] emission peaks. The contribution of the zodiacal light has been subtracted as explained in the text. The rotational lines of molecular hydrogen and the atomic fine-structure lines are labeled.

Cox et al. (see 495, L24)